Supporting Information

Gill et al. 10.1073/pnas.1423868112

SI Materials and Methods

Strain Construction and General Methods. All *B. subtilis* strains used in this study are derivatives of PY79 (1). Strains CVO1195 and CVO1395 (*amyE::spoVM-gfp cat* or *amyE::spoVM^{P9A}-gfp cat*) have been described previously (2). Strain CW245 (*amyE::spoVM^{R17D}-gfp cat*) was created by site-directed mutagenesis (QuikChange Kit; Agilent) using integration vector pKC2 (harboring *spoVM-gfp* under control of its native promoter, for insertion into the *amyE* locus (3)) as a template. *B. subtilis* competent cells were prepared as described previously (4). Plasmids pKR205 and pKR209 harboring *His6-SUMO-spoVM* and *His6-SUMO-spoVM^{P9A}*, respectively, under control of the T7 promoter were created by PCR amplifying either *spoVM* or *spoVM^{P9A}* with primers harboring abutted 5′ SapI and 3′ BamHI restrictions sites. PCR products were cloned into vector pTB146 (5) via 5′ SapI and 3′ BamHI sites. *B. subtilis* cells with GFP fusions were prepared for microscopy as described previously (6). Cells were viewed at room temperature with a DeltaVision Core microscope system (Applied Precision) equipped with a Photometrics CoolSNAP HQ2 camera. Planes were acquired every 200 nm, and the data were deconvolved using SoftWorx software.

SSLB Adsorption Assay.

Protein purification and labeling. SpoVM-GFP-His$_6$ or SpoVM^{P9A}-GFP-His$_6$ was overproduced in and purified from *Escherichia coli* BL21 harboring plasmids pKR155 or pKR167, respectively, as described previously (7). SpoVM-mini PEG-Cys was synthesized (Biomatik Corp.) and the C-terminal Cys residue was labeled with the maleimide derivative of Alexa Fluor 488 dye (Life Technologies) following the manufacturer's instructions.

SSLB preparation. SSLBs were made as described previously (8, 9). Briefly, liposomes were first produced by the sonication method using 100 μL (10 mg/mL) *E. coli* polar lipid extract (Avanti), which were first evaporated under vacuum overnight at room temperature onto the bottom of 16 × 100-mm borosilicate tubes, and hydrated in 500 μL ultrapure water. Resuspended lipids were then subjected to five cycles of freezing in a methanol/dry ice bath and thawing at 42 °C, followed by bath sonication for 35 min, or until the suspension became transparent. Debris was removed by centrifugation at 13,000 × *g* for 10 min, and the cleared supernatant, which contained unilamellar vesicles, was retained. Next, 10 mg of 2 μm-diameter silica beads (Polysciences, Inc.) or 8 μm-diameter silica beads (Cospheric LLC) were prepared for coating by washing three times in ultrapure water, followed by three washes in methanol and three washes in 1 M NaOH. After one additional wash in ultrapure water, the beads were resuspended in 200 μL of ultrapure water. Two hundred microliters of liposomes were then incubated with a 200-μL suspension of silica beads, and $CaCl_2$ was added to 1 μM final concentration. The suspension was vortexed for 2 min, then incubated at 42 °C for 30 min. After vortexing, SSLBs were collected by centrifugation at 13,000 × *g*, washed three times with ultrapure water, and resuspended in 1 mL 40 mM potassium phosphate at pH 7.5.

Microscopy. Varying concentrations of purified SpoVM-GFP, SpoVM^{P9A}-GFP, or synthesized SpoVM-Cys^{AF488} were incubated in 40 mM potassium phosphate at pH 7.5 (40 μL final reaction volume) containing 1 μL (10 mg/mL) 2-μm SSLBs, and 4 μL (10 mg/mL) 8-μm SSLBs to ensure equal surface area representation by both types of SSLBs. Binding reactions were incubated overnight at 25 °C following a program of alternating shaking and resting every 5 min to ensure that the beads did not settle. SSLB suspensions were placed on a glass-bottom culture dish (Mattek Corp.); a pad made of 1% agarose in distilled water was cut to size and placed above the SSLB suspension, as described previously (10), to prevent movement of the SSLBs. SSLBs were viewed at room temperature with a DeltaVision Core microscope system, and planes were acquired every 200 nm at room temperature; the data were deconvolved using SoftWorx version 6.1.1 (Applied Precision) as described above. The aggregate fluorescence intensities were then flattened onto a single plane, quantified using SoftWorx, and reported as fluorescence per square micron of SSLB surface area. The data were fit using an allosteric sigmoidal model [$y = B_{max}x^h/(K_{prime} + x^h)$], where B_{max} is adsorption extrapolated to very high concentration of substrate, h is the Hill coefficient, and $K_{prime} = K_{1/2}{}^h$, using Prism 5 software (GraphPad Software, Inc.).

Monte Carlo Simulations. In each simulation, to model the binding process of SpoVM molecules onto 2- and 8-μm beads, two sets of square lattices were initialized as empty to represent available binding sites on the beads. The 2-μm beads were represented by sixteen 20 × 20 lattices, and an 8-μm bead was represented by a single 80 × 80 lattice, so that there was an equal fraction of binding sites on each bead size. All lattices had the same spacing and had periodic boundary conditions. In the absence of cooperativity, during each time step dt, an empty site on a 2- or 8-μm bead became bound with probability $k_{2\_on}N_{unbound}dt$ or $k_{8\_on}N_{unbound}dt$, respectively, where $N_{unbound}$ is the number of unbound SpoVM molecules. To represent cooperativity in binding when a site was occupied by a SpoVM molecule, the probability for SpoVM binding to its four nearest-neighbor sites was increased by a factor $\exp(E_c)$. The probability for a bound SpoVM to be released was determined by off rates $k_{2\_off} = k_{8\_off}$. For the simulations in Fig. 2, $k_{2\_on} = 1$ and $k_{2\_off} = 5{,}000$. The time step was chosen to be sufficiently small so that all probabilities were $\ll 1$. Simulations were terminated when the density of molecules bound to the 2- and 8-μm beads had reached a steady-state value.

Molecular Dynamics Simulations. Molecular dynamics simulations were carried out on the special-purpose Anton supercomputer (11) and analyzed with the software VMD (12). Interactions between atoms were characterized with the CHARMM27 force field for protein (13, 14), CHARMM36 force field for lipids (15), and the TIP3P model for water (16). Protein structures were initialized with the NMR structures solved in this study, and each was placed on a 1,2-dioleoyl-*sn*-glycero-3-phosphocholine membrane patch. Water molecules and neutralizing ions were added above and below the bilayer, and in sum each simulation contained ~91,000 atoms. After equilibrating the membrane–protein systems with the software NAMD (17), simulations were conducted on Anton in the NPT ensemble at 310 K and 1 atm. Periodic boundary conditions were used, and the integration time step was 2 fs. The membrane–protein system with SpoVM^{WT} was simulated for ~3,900 ns, and the SpoVM^{P9A} simulation was conducted for ~2,600 ns. Analyses of the trajectories involved the last 500 ns of each simulation to ensure the proteins were fully stabilized in the membrane.

NMR Spectroscopy.

Preparation of isotopic-labeled proteins. His$_6$-Sumo-SpoVM and His$_6$-Sumo-SpoVM^{P9A} were overproduced in and purified from *E. coli* BL21 (DE3) harboring plasmids pKR205 or pKR209, respectively. Briefly, LB starter cultures for *E. coli* BL21 (DE3) pKR205 pRIL were inoculated with 100 μg/mL ampicillin and

25 μg/mL chloramphenicol for plasmid maintenance. LB starter cultures of *E. coli* BL21 (DE3) Gold pKR209 were inoculated with 100 μg/mL ampicillin. Starter cultures were grown at 37 °C for 12 h. Recombinant proteins were typically produced by inoculating 250 mL M9 medium with 50:1 LB starter culture and inducing expression of the fusion protein at an optical density at 600 nm of 0.6–0.9 with 1 mM isopropyl β-D-1-thiogalactopyranoside at 16 °C for ∼20 h. M9 medium was supplemented with $^{15}NH_4Cl$ (1 g/L) for ^{15}N-labeled samples or D-glucose-$^{13}C_6$ (4 g/L) and $^{15}NH_4Cl$ (1 g/L) for $^{15}N/^{13}C$-labeled samples. Cells were harvested by centrifugation and the pellets were stored at −80 °C until use.

Cell pellets were homogenized with a lysis buffer of 50 mM phosphate [pH 7.4] and 500 mM NaCl, and were lysed using a French press at 1,500 psi (single pass) followed by sonication on ice for 5-s on/5-s off intervals for 3 min total duration. Cell debris was removed by centrifugation at 15,000 × *g* at 10 °C for 20 min. Supernatants were collected and 0.8% dodecyl maltoside (DM; final concentration) and 30 mM imidazole were added to solubilize cell membranes. After agitating at room temperature for 1 h, the supernatant was applied twice to Ni-NTA columns. The columns were washed with 40 mL lysis buffer containing 40 mM imidazole and 0.2% DM. Proteins were eluted with an elution buffer of 20 mM Tris·HCl [pH 8.0], 500 mM NaCl, 500 mM imidazole, and 0.4% DM into tubes with equal volumes of 20 mM Tris [pH 8.0] and 0.4% DM solution to reduce the concentrations of NaCl and imidazole for the following step.

The N-terminal His_6-Sumo tag was removed by addition of H-Ulp1-His_6-Sumo protease to the above elution at a mass ratio of 5:1 (protein:protease) for overnight agitation at 25 °C. Complete cleavage of the tag was confirmed by SDS/PAGE. After diluting the imidazole from 250 mM to 50 mM with a buffer of 20 mM Tris [pH 8.0], the sample was reapplied to an Ni-NTA column and washed first with a buffer of 20 mM Tris·HCl [pH 8.0], 500 mM NaCl, 80 mM guanidine-HCl, and 0.8% DM and then a buffer of 20 mM Tris·HCl [pH 8.0], 2 M NaCl, 80 mM guanidine-HCl, and 0.8% DM. Both washes contained the target protein and were combined and concentrated. Following detergent removal by either extensive dialysis or repeated exchange with an Amicon Ultra centrifugal filter device (Millipore), the protein was reconstituted into a 16% 1,2-dimyristoyl-*sn*-glycero-3-phosphocholine (DMPC)/1,2-dihexanoyl-*sn*-glycero-3-phosphocholine (DHPC) (q = 0.3) bicelle solution with 80 mM NaCl and 16 mM phosphate at pH 6.0. For ^{13}C-edited experiments, deuterated DMPC and DHPC lipids were used. Typical NMR sample concentrations were between 0.5 and 1 mM.

Resonance assignment, structure determination, dynamics, and PRE measurements. All NMR data were acquired at 37 °C on Bruker 600- or 850-MHz spectrometers equipped with cryoprobes. The data were processed using NMRPipe and analyzed using NMRView. Backbone resonance assignments were carried out using TROSY-based triple resonance HNCA, HN(CO)CA, HNCACB, and HN(CO)CACB experiments. Side-chain resonance assignments were obtained from the 3D ^{13}C-edited HCCHTOCSY experiment. Distance constraints for NMR structure determination were derived from 3D ^{15}N-edited and ^{13}C-edited NOESYHSQC data. NOE assignments were obtained by a combined manual and automated analysis with CYANA 3.0. Torsion angle constraints were derived from C^{α}, C^{β}, N, and C' chemical shifts using TALOS+ (18). The structures were calculated using XPLOR-NIH. PROCHECK-NMR was used to analyze the 10 lowest-energy structures (Table S1). Backbone ^{15}N relaxation data and $^{1}H_N$ PREs were collected on ^{15}N-labeled samples. The ^{15}N longitudinal relaxation rates (R_1) were determined from the data with relaxation delays of 50, 150, 250, 350, 500, 650, 750, 950, and 1,300 ms. The transverse relaxation rates (R_2) were determined from the data with relaxation delays of 16.1, 32.3, 48.4, 64.5, 80.7, 96.8, and 113 ms. The steady-state heteronuclear ^{15}N-{^{1}H} NOEs were determined from peak ratios between two spectra collected with a 3-s presaturation on or off in the proton channel proceeded by a 6-s recycle delay. To measure PREs, Gd(DTPA) was titrated to protein samples from a stock solution of 178 mM Gd(DTPA) and 310 mM EDTA, or 16-DSA was titrated to protein samples from a stock solution of 50 mM 16-DSA in 16% bicelle solution. $^{1}H_N$ R_2 rates were determined using a 2D TROSY-based experiment similar to one previously described (19).

1. Youngman P, Perkins JB, Losick R (1984) Construction of a cloning site near one end of Tn917 into which foreign DNA may be inserted without affecting transposition in *Bacillus subtilis* or expression of the transposon-borne *erm* gene. *Plasmid* 12(1):1–9.
2. van Ooij C, Losick R (2003) Subcellular localization of a small sporulation protein in *Bacillus subtilis*. *J Bacteriol* 185(4):1391–1398.
3. Ramamurthi KS, Clapham KR, Losick R (2006) Peptide anchoring spore coat assembly to the outer forespore membrane in *Bacillus subtilis*. *Mol Microbiol* 62(6):1547–1557.
4. Wilson GA, Bott KF (1968) Nutritional factors influencing the development of competence in the *Bacillus subtilis* transformation system. *J Bacteriol* 95(4):1439–1449.
5. Bendezú FO, Hale CA, Bernhardt TG, de Boer PA (2009) RodZ (YfgA) is required for proper assembly of the MreB actin cytoskeleton and cell shape in *E. coli*. *EMBO J* 28(3):193–204.
6. Eswaramoorthy P, et al. (2011) Cellular architecture mediates DivIVA ultrastructure and regulates min activity in *Bacillus subtilis*. *MBio* 2(6):e00257-11.
7. Ramamurthi KS, Lecuyer S, Stone HA, Losick R (2009) Geometric cue for protein localization in a bacterium. *Science* 323(5919):1354–1357.
8. Bayerl TM, Bloom M (1990) Physical properties of single phospholipid bilayers adsorbed to micro glass beads. A new vesicular model system studied by 2H-nuclear magnetic resonance. *Biophys J* 58(2):357–362.
9. Gopalakrishnan G, Rouiller I, Colman DR, Lennox RB (2009) Supported bilayers formed from different phospholipids on spherical silica substrates. *Langmuir* 25(10):5455–5458.
10. Eswaramoorthy P, et al. (2014) Asymmetric division and differential gene expression during a bacterial developmental program requires DivIVA. *PLoS Genet* 10(8):e1004526.
11. Shaw DE, et al. (2008) Anton, a special-purpose machine for molecular dynamics simulation. *Commun ACM* 51(7):91–97.
12. Humphrey W, Dalke A, Schulten K (1996) VMD: Visual molecular dynamics. *J Mol Graph* 14(1):33–38, 27–28.
13. Mackerell AD, Jr, Feig M, Brooks CL, 3rd (2004) Extending the treatment of backbone energetics in protein force fields: Limitations of gas-phase quantum mechanics in reproducing protein conformational distributions in molecular dynamics simulations. *J Comput Chem* 25(11):1400–1415.
14. MacKerell AD, Jr, et al. (1998) All-atom empirical potential for molecular modeling and dynamics studies of proteins. *J Phys Chem B* 102(18):3586–3616.
15. Klauda JB, et al. (2010) Update of the CHARMM all-atom additive force field for lipids: validation on six lipid types. *J Phys Chem B* 114(23):7830–7843.
16. Jorgensen WL, Chandrasekhar J, Madura JD, Impey RW, Klein ML (1983) Comparison of simple potential functions for simulating liquid water. *J Chem Phys* 79:926–935.
17. Phillips JC, et al. (2005) Scalable molecular dynamics with NAMD. *J Comput Chem* 26(16):1781–1802.
18. Shen Y, Delaglio F, Cornilescu G, Bax A (2009) TALOS+: A hybrid method for predicting protein backbone torsion angles from NMR chemical shifts. *J Biomol NMR* 44(4):213–223.
19. Iwahara J, Tang C, Marius Clore G (2007) Practical aspects of (1)H transverse paramagnetic relaxation enhancement measurements on macromolecules. *J Magn Reson* 184(2):185–195.

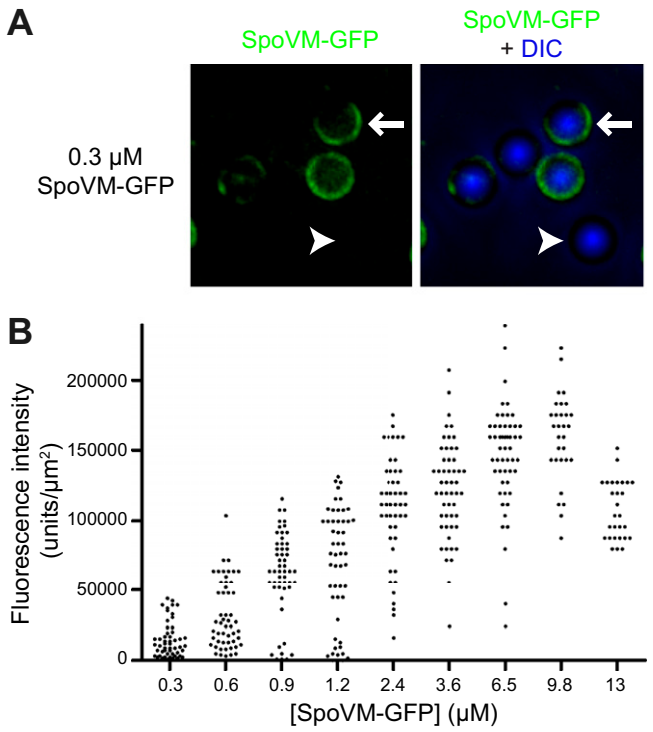

Fig. S1. Fluorescence intensities of SSLBs bound with purified SpoVM-GFP. (*A*) Magnified view from Fig. 1*C*, far left panels, showing the nonuniform distribution of SpoVM-GFP fluorescence on 2-μm beads at 0.3 mM concentration. As in Fig. 1, arrow indicates a bead with a nonuniform fluorescence pattern; arrowhead indicates a bead with little or no fluorescence. (*B*) Quantification of mean fluorescence intensities (arbitrary units per micron) for individual SSLBs incubated with varying concentrations of purified SpoVM-GFP. Each data point represents the fluorescence intensity from a single SSLB.

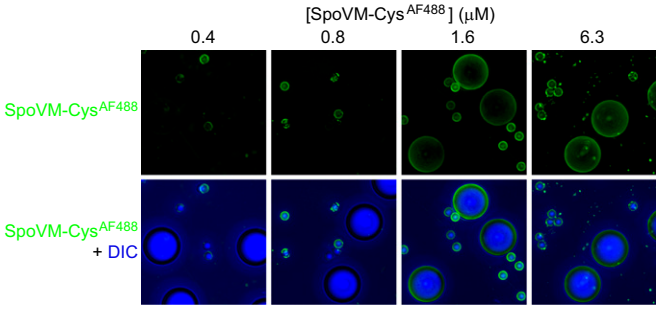

Fig. S2. SpoVM-Cys labeled with a fluorescent dye preferentially localizes to membranes with higher curvature. Fluorescence micrographs of SSLBs, either 2 or 8 μm in diameter, incubated with increasing concentrations of synthesized SpoVM derivatized with a mini-PEG tag followed by Cys conjugated with the fluorescent dye Alexa Fluor 488. (*Upper*) Aggregate fluorescence across several z-stacks is depicted in green; (*Lower*) overlay of fluorescence (green); and SSLBs visualized by DIC (blue).

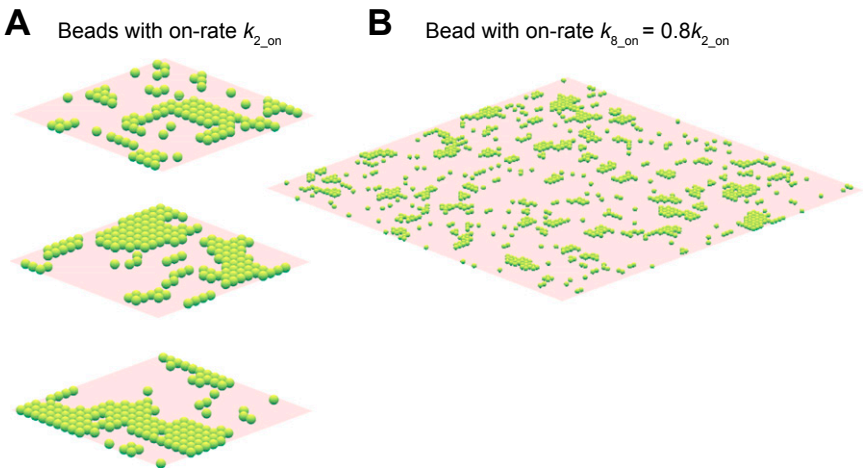

Fig. S3. Clusters of SpoVM molecules in Monte Carlo simulations. (*A*) The spatial distribution of SpoVM molecules (shown as green spheres) at steady state on three representative examples of periodic 20 × 20 square lattices (shown as red plane) representing the surfaces of 2-μm SSLBs, for a Monte Carlo simulation (*SI Materials and Methods*) used to generate Fig. 2 with $E_c = 2k_BT$, $k_{2\_on} = 1$ (in arbitrary time units), $k_{8\_on} = 0.2k_{2\_on}$, and 3,000 total SpoVM molecules. (*B*) The spatial distribution of SpoVM molecules on a periodic 80 × 80 square lattice representing the surface of an 8-μm SSLB for the same simulation in *A*. The surfaces in *A* have higher densities of bound molecules, and exhibit spatial heterogeneity qualitatively similar to our experimental measurements of binding to 2-μm beads incubated with 0.3 mM SpoVM-GFP shown in Fig. S1*C*.

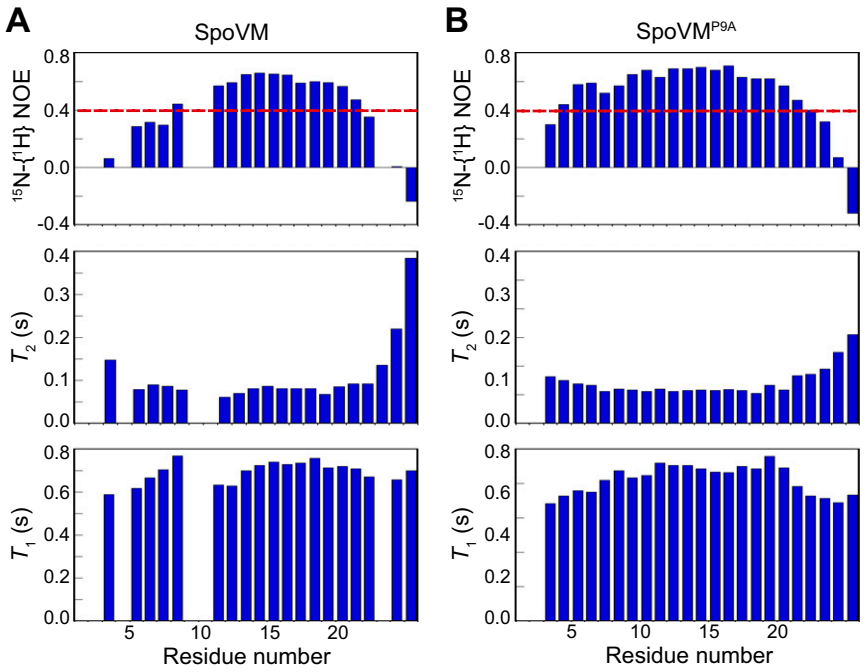

Fig. S4. NMR relaxation experiments performed on SpoVM and SpoVM^{P9A}. (*A*) Backbone steady-state heteronuclear ^{15}N-{^{1}H} NOEs and amide ^{15}N T_2 and T_1 relaxation times for (*A*) SpoVM or (*B*) SpoVM^{P9A} in isotropic DMPC/DHPC bicelles.

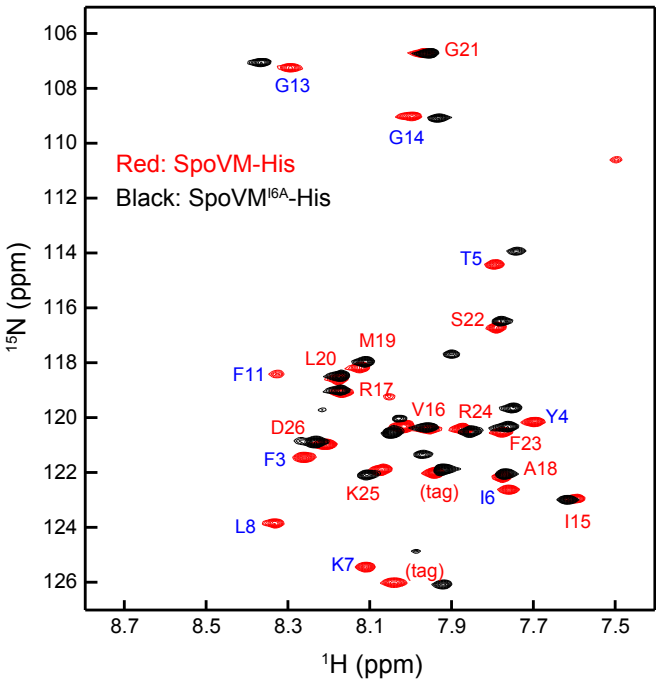

Fig. S5. Overlay of ^{1}H-^{15}N TROSY spectra of SpoVM-His$_6$ and SpoVM^{I6A}-His$_6$ in isotropic bicelles. Resonances with substantial shifts are labeled in blue and others are colored in red.

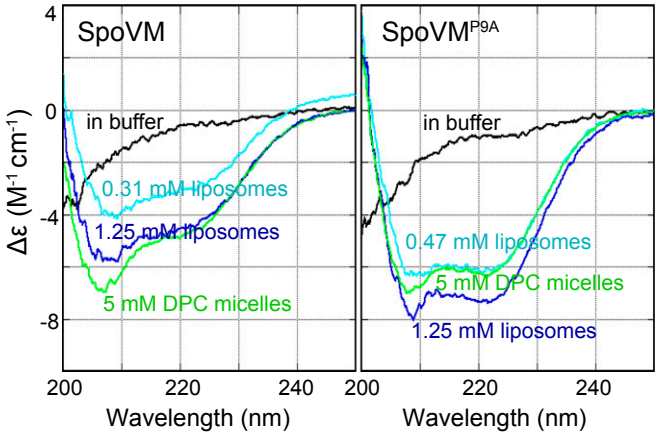

Fig. S6. Circular dichroism spectra of SpoVM and SpoVM^{P9A} in DMPC liposomes and DPC micelles. CD spectra of SpoVM (*Left*) or SpoVM^{P9A} (*Right*), determined in buffer (black), DMPC liposomes at the concentrations indicated (light blue and dark blue), or DPC micelles (green).

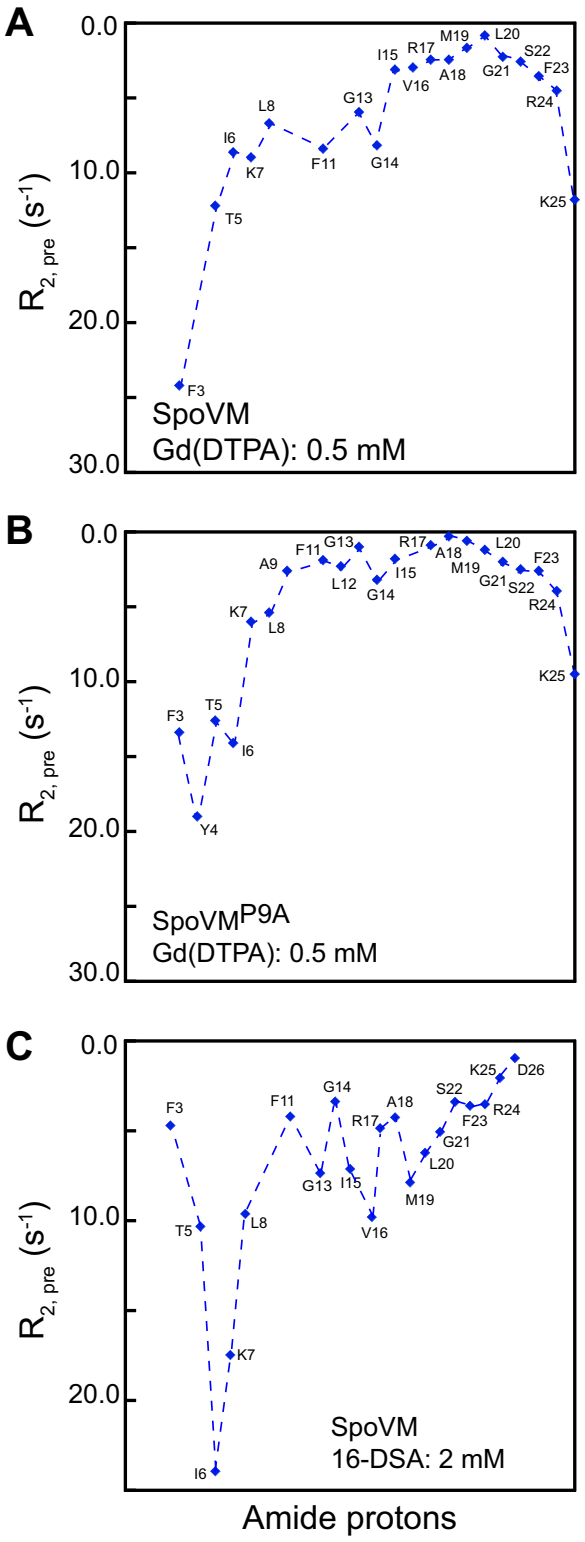

Fig. S7. Orientation and insertion depth of SpoVM and SpoVM^{P9A} in the membrane. PRE effects on (*A*) SpoVM with 0.5 mM Gd(DTPA), (*B*) SpoVM^{P9A} with 0.5 mM Gd(DTPA), and (*C*) SpoVM with 2 mM 16-DSA. The large PRE effects for the N-terminal residues are likely due to the flexibility of the SpoVM N-terminal loop.

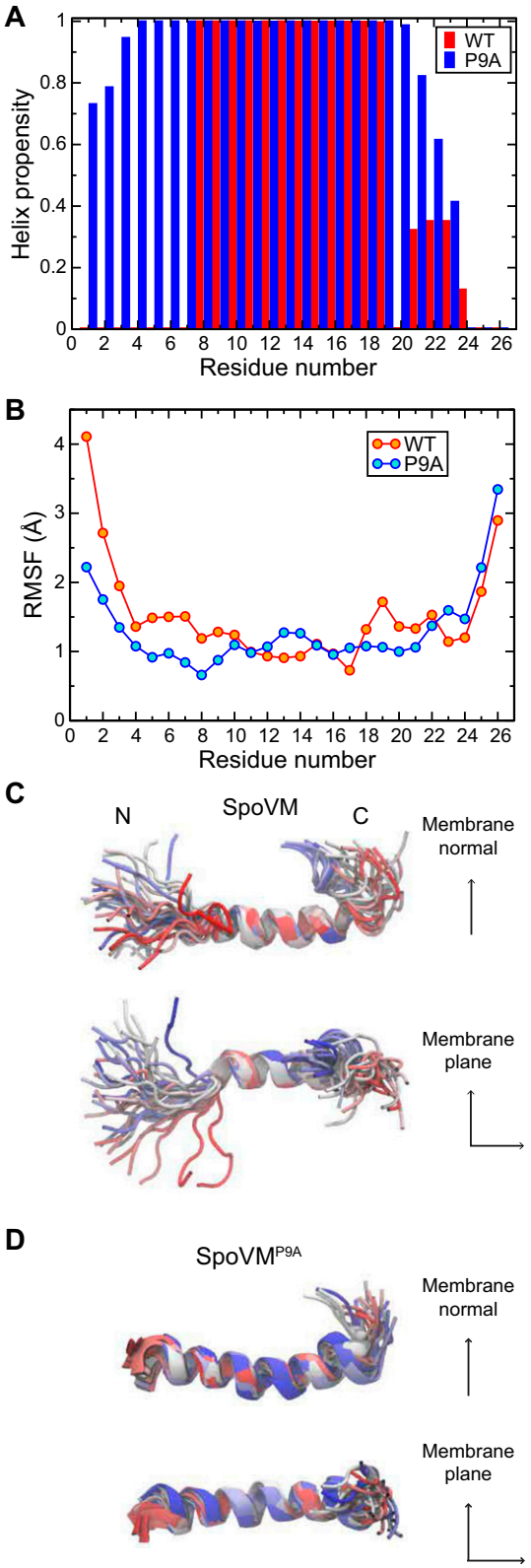

Fig. S8. MD simulations of the structures of SpoVM and SpoVM^{P9A} in the membrane. (*A*) Calculated probability of each amino acid in SpoVM (red) or SpoVM^{P9A} (blue) to form an α-helix. (*B*) Rms fluctuation of each amino acid in SpoVM (red) or SpoVM^{P9A} (blue), as a measurement of flexibility. (*C* and *D*) Structures of (*C*) SpoVM or (*D*) SpoVM^{P9A} observed during the simulations in Fig. 5 and Movies S1 and S2, colored according to simulation time (red, beginning of the simulation; blue, end of the simulation).

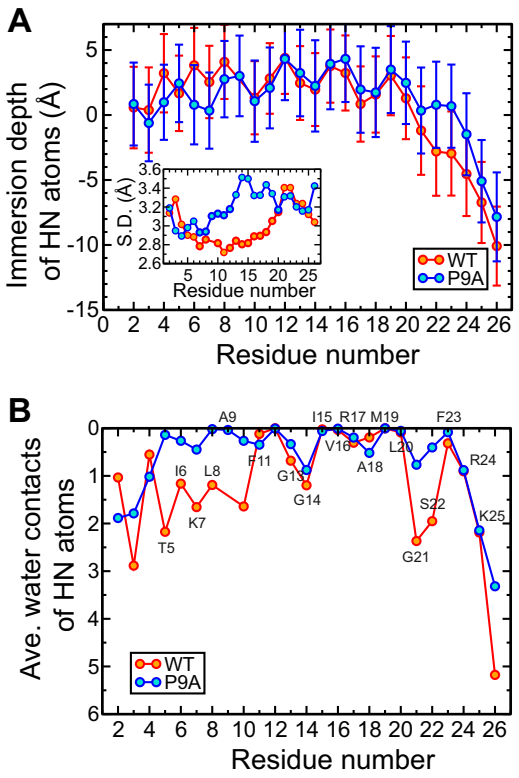

Fig. S9. Average insertion depth of SpoVM and SpoVM^{P9A} as determined by MD simulations. (*A*) Immersion depth of the amide proton in each applicable amino acid in SpoVM (red) or SpoVM^{P9A} (blue). Error bars are SDs. (*Inset*) SD of each data point, demonstrating that for wild-type SpoVM, fluctuations in immersion depth are more prominent at the termini. (*B*) Solvent accessibility of each amino acid in SpoVM (red) or SpoVM^{P9A} (blue), approximated by measuring the average number of water molecules within 4 Å of the amide proton.

Table S1. NMR constraints and structure statistics for SpoVM and SpoVM^{P9A}

Structure parameters	SpoVM	SpoVM^{P9A}
NMR constraints		
NOE distances	391	365
Intraresidue	96	100
Sequential ($\|i - j\| = 1$)	126	121
Medium range ($2 \leq \|i - j\| \leq 4$)	160	144
Long range ($\|i - j\| \geq 5$)	12	0
Dihedral angles		
Phi	10	16
Psi	10	16
Structure statistics		
Rmsd from the average atomic coordinates*		
Backbone, Å	0.2	0.3
Heavy, Å	0.8	0.7
Ramachandran analysis*		
Most favored	90%	99.4%
Additionally allowed	10%	0.6%
Generally allowed	0.0	0.0
Disallowed	0.0	0.0
Violations (mean ± SD)		
Distance constraints, Å	0.075 ± 0.004	0.070 ± 0.004
Dihedral angle constraints, °	0.721 ± 0.144	0.307 ± 0.170
Deviations from idealized geometry		
Bond lengths, Å	0.009 ± 0.000	0.008 ± 0.000
Bond angles, °	0.836 ± 0.019	0.720 ± 0.021
Improper, °	0.525 ± 0.045	0.449 ± 0.033

*Evaluated by PROCHECK for ordered residues, 11–23 of SpoVM and 3–23 of SpoVM^{P9A}.

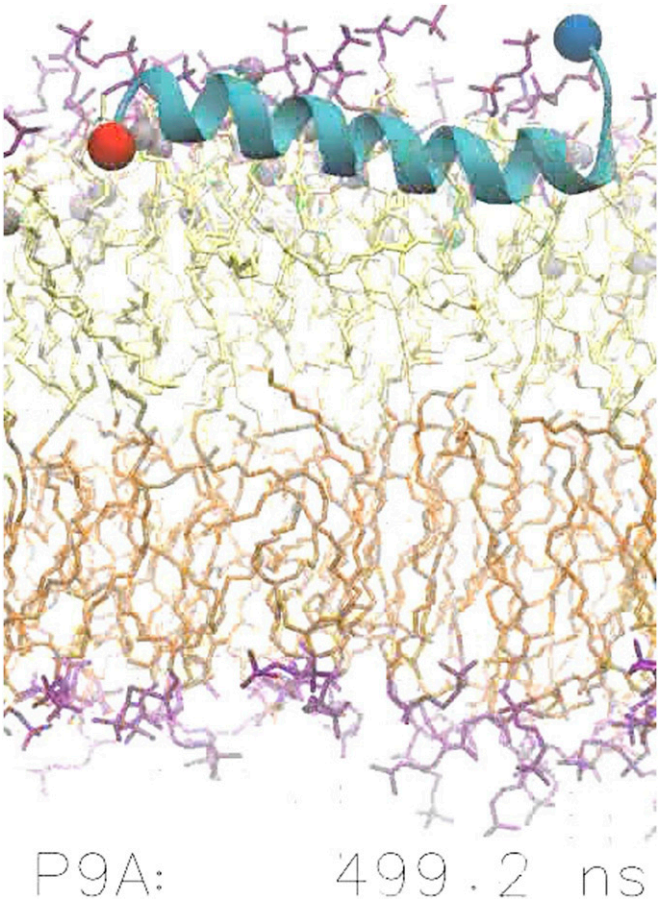

Movie S1. Molecular dynamics simulation of a single molecule of SpoVM.

Movie S1

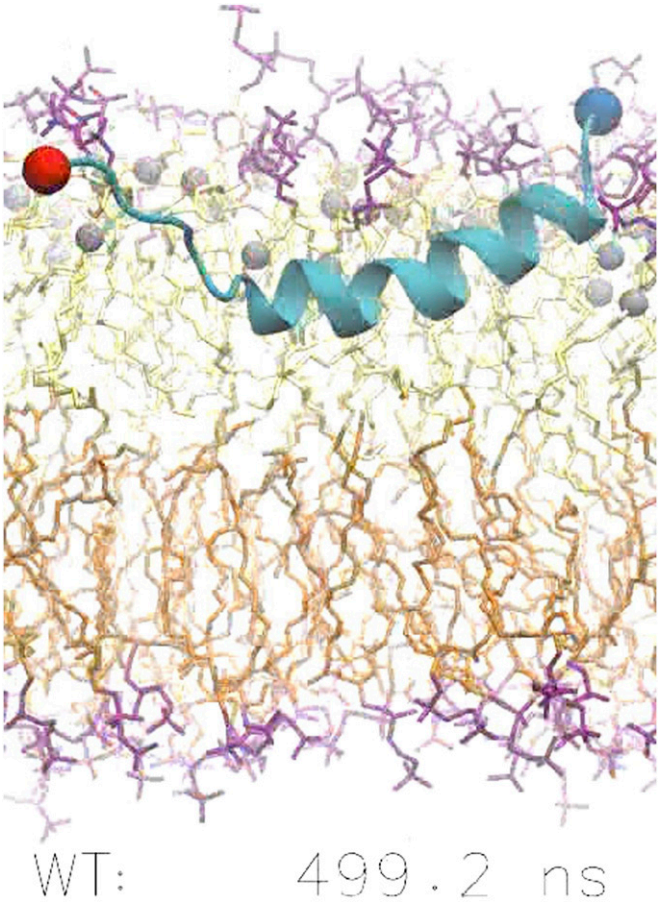

Movie S2. Molecular dynamics simulation of a single molecule of SpoVM^{P9A}.

Movie S2